ACS Catalysis

Letter

pubs.acs.org/acscatalysis

Octahedral Pt_2CuNi Uniform Alloy Nanoparticle Catalyst with High Activity and Promising Stability for Oxygen Reduction Reaction

Changlin Zhang, William Sandorf, and Zhenmeng Peng*

Department of Chemical and Biomolecular Engineering, The University of Akron, Akron, Ohio 44325, United States

Supporting Information

ABSTRACT: Development of a highly active and stable electrocatalyst is of great significance in the oxygen reduction reaction (ORR) research. Although octahedral Pt−Ni nanoparticle catalysts have attracted much interest because of their high activity, their poor stability raises a severe issue for real applications. We achieve both outstanding ORR activity and much improved catalyst stability by preparing octahedral Pt_2CuNi alloy nanoparticles with uniform element distribution, with the activity far exceeding the DOE target and the stability comparable to that of state-of-the-art Pt/C. The improved stability is attributed to uniform elemental distribution within the ternary particles, which helps with formation of intact Pt surface layers and good retention of the octahedral morphology.

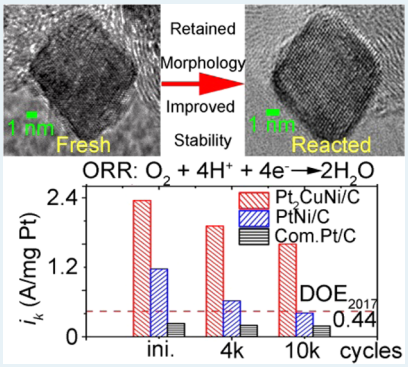

KEYWORDS: *oxygen reduction reaction, electrocatalyst, octahedral nanoparticle, activity, stability*

The big cost of oxygen reduction reaction (ORR) catalyst is a huge hurdle for the polymer electrolyte membrane fuel cell (PEMFC) technology.[1,2] The discovery that single crystalline Pt_3Ni (111) exhibits exceptionally high ORR activity (18 mA/cm^2 Pt at 0.9 V vs RHE), which is about 90 times the activity of commercial Pt/C, points to an ideal strategy for solving the cost problem by using Pt alloy nanoparticle catalyst with both finely controlled particle composition and surface facet.[3] Thereafter, many research efforts have been devoted to preparing such nanosized catalysts and studying the property. For example, several research groups have successfully synthesized octahedral Pt−Ni alloy nanoparticles, which possess a (111) facet and a large specific surface, and achieved high area-specific and mass ORR activities, demonstrating good promise of the strategy.[4−9] However, one remaining problem of these particular nanoparticle catalysts is their poor stability. The ORR activity, accompanied by fast leaching of Ni element and collapse of particle morphology, decays rapidly, within thousands of potential sweeping cycles.[6] It makes these catalysts insufficient for the long-term operation requirement for real applications.[2,6] Thus, how to improve the stability of the shaped nanoparticles and retain their high activity becomes crucial in the ORR catalyst research.

Herein, we report the preparation of octahedral Pt_2CuNi alloy nanoparticle catalyst, which, benefiting from atomic level uniformity of the particle composition, exhibits both high ORR activity and much improved stability compared with the Pt−Ni counterparts. The octahedral Pt_2CuNi nanoparticles on carbon support (Pt_2CuNi/C, 20 wt % Pt) was produced with a modified solid-state chemistry method (see Supporting Information (SI) for details), in which H_2 functions as reducing agent for the metal precursors and CO helps to shape growing particles into octahedrons.[10−12] As shown in the transmission electron microscopy (TEM) image (Figure 1A), the prepared Pt_2CuNi nanoparticles were well dispersed on the C support. Statistical analyses of more than 200 particles show that about 80% of the particles were in an octahedral morphology, demonstrating the effectiveness of the solid-state chemistry method in producing octahedral Pt_2CuNi. The octahedral Pt_2CuNi had a narrow size distribution, with a measured average edge length of 8.1 ± 0.4 nm (Figure 1A and SI Figure S1). Figure 1B shows high-resolution TEM (HRTEM) of individual Pt_2CuNi nanoparticles, which had straight edges and clear lattice fringes. The lattice spacing was measured to be 2.18 Å, which is significantly smaller than that of face-centered cubic (fcc) Pt (111) (2.27 Å) and indicates the formation of alloy structure.[5,12] The high-angle annular dark field scanning TEM (HAADF-STEM) image and the corresponding energy dispersive X-ray (EDX) elemental mappings are shown in Figure 1C−F. All three elements were found with a distribution throughout the whole particle and were of similar map size, suggesting the octahedral Pt_2CuNi is in its ternary alloy phase. The average particle composition was determined to be $Pt_{50}Cu_{26}Ni_{24}$ using quantitative EDX measurements and the metal loading in the final product was determined to be 21.0% using thermal gravity (TG) analyses, both of which were consistent to the stoichiometry of precursors (Table 1, SI Figure S2 and S3). The X-ray diffraction (XRD) pattern confirmed an fcc structure for the ternary particles and showed

Received: December 29, 2014
Revised: February 17, 2015
Published: March 9, 2015

DOI: 10.1021/cs502112g
ACS Catal. 2015, 5, 2296−2300

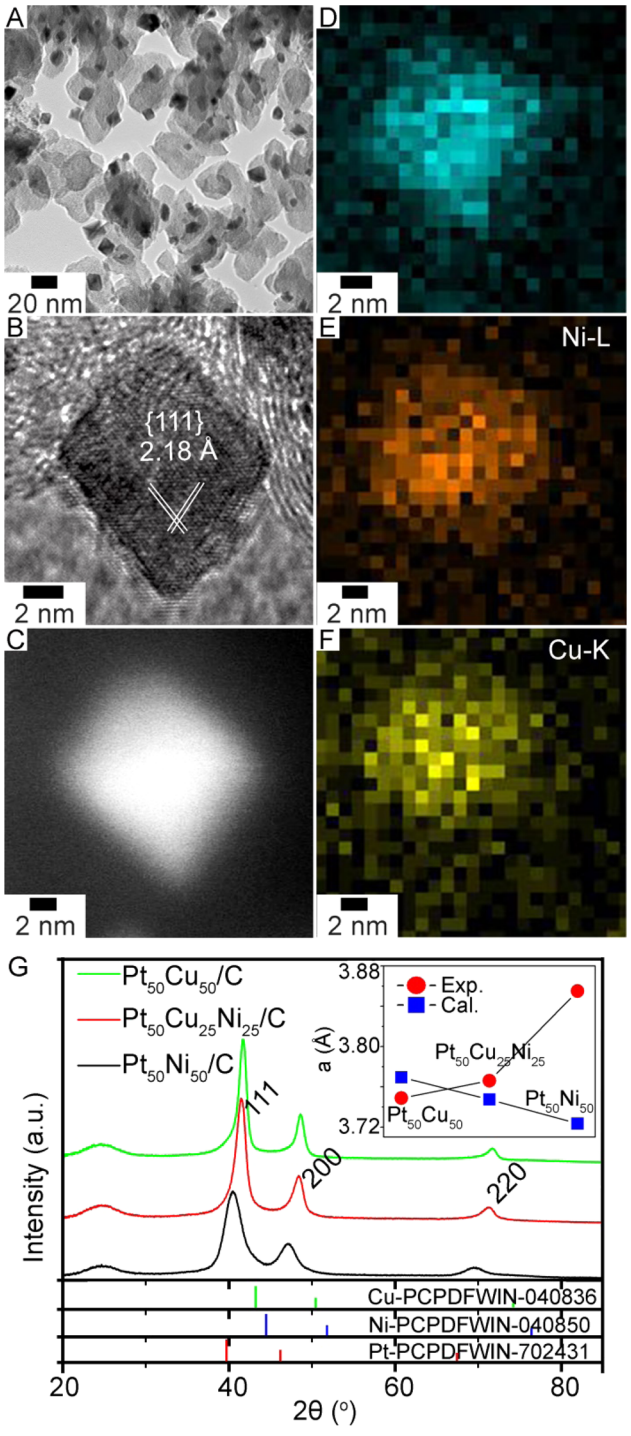

Figure 1. (A) TEM, (B) HRTEM, (C) HAADF-STEM, and (D–F) EDX elemental maps of as-prepared Pt_2CuNi/C, and (G) XRD of as-prepared Pt_2CuNi/C, PtNi/C, and PtCu/C, with reference peaks for pure Cu, Ni, and Pt being included for comparison and with inset showing calculated and experimental lattice parameters.

characteristic peak shifts comparing to that for their pure components due to the alloy formation (Figure 1G). The lattice parameter determined from the (111) diffraction peak using Bragg's law was 3.77 Å. It was close to the value (3.75 Å), calculated from the particle composition using Vegard's law, which predicts lattice parameter of uniform alloys.[13] The good agreement indicates an uniform alloy composition of the Pt_2CuNi. In other words, all three elements have even distributions at atomic level within individual Pt_2CuNi nanoparticles.

PtNi/C and PtCu/C nanoparticles were prepared using the same method and with the same Pt content for direct comparison purpose. The produced PtNi nanoparticles had an octahedral morphology, in consistence with our previous studies, whereas most of the PtCu particles were polyhedral (SI Figure S4).[12] Mechanistic investigations have attributed the formation of octahedral Pt–Ni to surface-dependent CO adsorption. The Pt–Ni (111) has the strongest interaction with CO compared with other facet planes. It causes the slowest growth rate of the (111) planes, which consequently become the exposure surface and confine the particle growth into octahedral morphology.[10,12] The formation mechanism of octahedral Pt_2CuNi could be similar to that of octahedral Pt–Ni. The inability to control the shape of PtCu nanoparticles was associated with the weak CO adsorption to Cu and the high Cu content, which caused low CO coverage on the growing particles and thus bad control over the surface formation.[14] The two samples were characterized in parallel to the octahedral Pt_2CuNi/C (Table 1, Figures S2–S4). An interesting finding with the octahedral PtNi/C was the big discrepancy between the lattice parameter obtained using Bragg's law (3.86 Å) and using Vegard's law (3.72 Å) (Figure 1G).[15,16] It indicated that Pt and Ni atoms distributed nonuniformly within the octahedral PtNi nanoparticles and had elemental segregations. The finding agreed with previous electron energy loss spectroscopy (EELS) studies,[6] which found Ni enrichment in particle terrace regions and Pt segregation to particle edges. On the other side, the PtCu/C had matched lattice parameter calculated from Bragg's law and Vegard's law (3.75 Å vs 3.77 Å), suggesting an even distribution of Cu and Pt elements within the particles.[17] The more uniform alloy composition of PtCu than PtNi can be originated from their different segregation energy (E_{segr}).[18] Computational studies show a negative E_{segr} for the Pt–Ni system, which drives Pt to segregate from Ni. The Pt–Cu system has an E_{segr} near to zero, which favors atomic level mixing of the two metals.[18] The uniform elemental distribution within the octahedral Pt_2CuNi/C benefits from the Cu addition. The presence of Cu can effectively decrease the system E_{segr}, which mitigates elemental segregation between Pt and Ni and largely improves the alloy uniformity.

Electrochemical measurements were conducted for studying the ORR property of the prepared catalysts, with the linear sweep voltammetry (LSV) data shown in Figure 2A. The octahedral Pt_2CuNi/C exhibited the most positive half-wave potential ($E_{1/2}$) and had a 70 mV shift compared with the commercial Pt/C (20 wt % Pt), implying dramatically improved reaction kinetics.[19] The area-specific ORR current densities ($i_{k,\,area}$), a descriptor for electrocatalyst intrinsic activity, were calculated and compared (Figure 2B and Table 1). All four samples were observed with comparable Tafel slopes, suggesting the same ORR pathways on these catalysts. The Pt_2CuNi/C exhibited 6.65 mA/cm^2 Pt at 0.90 V versus RHE, which was around 30 times of 0.23 mA/cm^2 Pt using the commercial Pt/C. The value was also significantly higher than that for the octahedral PtNi/C and the PtCu/C and was among the highest $i_{k,\,area}$ ever reported (see Table S1).[20–30]

Previous studies have discovered that the d-band center (ε_d) of surface Pt can be shifted downward under electronic interaction with both Ni and Cu, which promotes ORR by suppressing competitive hydroxyl species adsorption on the

DOI: 10.1021/cs502112g
ACS Catal. 2015, 5, 2296–2300

Table 1. Physical Parameters and ORR Property of Octahedral Pt_2CuNi/C, Octahedral PtNi/C, PtCu/C, and Commercial Pt/C

catalysts		Pt/C	PtNi/C	Pt_2CuNi/C	PtCu/C
composition:[a] as-prepared			$Pt_{52}Ni_{48}$	$Pt_{50}Cu_{26}Ni_{24}$	$Pt_{50}Cu_{50}$
composition: initial			$Pt_{74}Ni_{26}$	$Pt_{57}Cu_{25}Ni_{18}$	$Pt_{56}Cu_{44}$
composition: 4k cycles			$Pt_{82}Ni_{18}$	$Pt_{62}Cu_{24}Ni_{14}$	$Pt_{61}Cu_{39}$
composition: 10k cycles			$Pt_{83}Ni_{17}$	$Pt_{64}Cu_{24}Ni_{12}$	N/A
$i_{k,\ area}$ (mA/cm^2 Pt) @ 0.90 V	initial	0.23	2.26	6.65	2.61
	4k cycles	0.22	1.54	5.19	1.93
	10k cycles	0.23	0.94	4.78	N/A
$i_{k,\ mass}$ (A/mg Pt) @ 0.90 V	initial	0.21	1.17	2.35	0.72
	4k cycles	0.18	0.62	1.91	0.49
	10k cycles	0.17	0.41	1.60	N/A

[a]Determined by EDX.

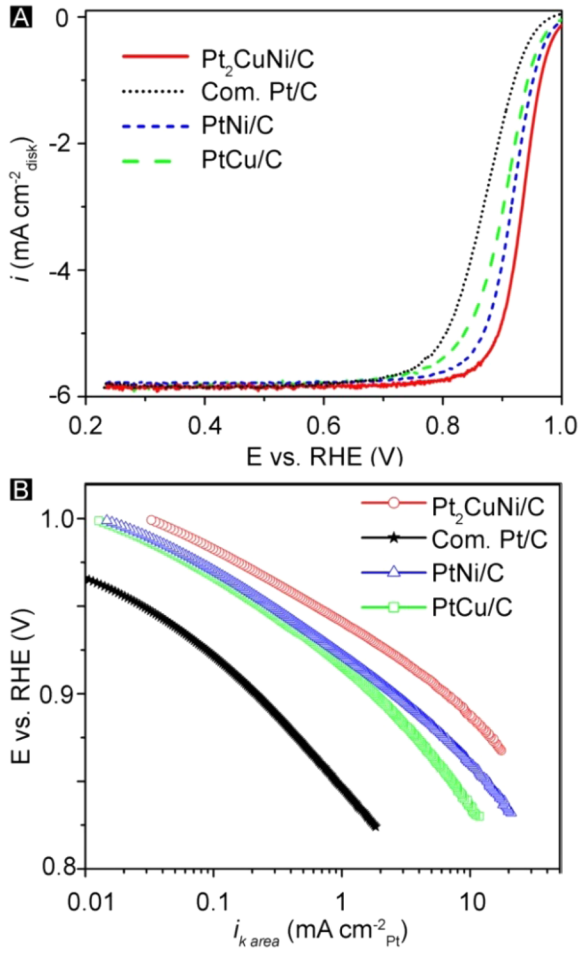

Figure 2. (A) ORR polarization curves in O_2-saturated 0.1 M $HClO_4$ electrolyte and (B) Tafel plots for the octahedral Pt_2CuNi, octahedral PtNi, PtCu, and commercial Pt catalysts.

surface.[4,6,31−34] Besides, intactness of the (111) surface plane can also help with decreasing surface coverage of adsorbed hydroxyl species. The much improved ORR kinetics on the octahedral Pt_2CuNi can thus be attributed to combinational electronic and geometric effects. Meanwhile, less Pt content of the Pt_2CuNi than most Pt−Ni nanoparticle catalysts benefits the catalyst with higher ORR mass activity and more efficient utilization of the precious metal. With an electrochemical active surface area (ECSA) of 35.3 m^2/g Pt, the mass activity ($i_{k,\ mass}$) of the Pt_2CuNi/C was determined to be 2.35 A/mg Pt at the potential, which was about 11 times more active than the commercial Pt/C and five times of the DOE 2017 target value (0.44 A/mg Pt).[1]

The stability of the Pt_2CuNi/C was evaluated by potentially cycling the catalyst electrode at 50 mV/s between 0.6 and 1.0 V for 4000 cycles in 0.1 M $HClO_4$, a standard protocol used in literature.[35] The recorded cyclic voltammograms (CV) before and after the test are shown in Figure 3A. A slight 4.4% increase in the ECSA was observed, which was associated with surface roughing of the particles during the test.[36] The degradation in

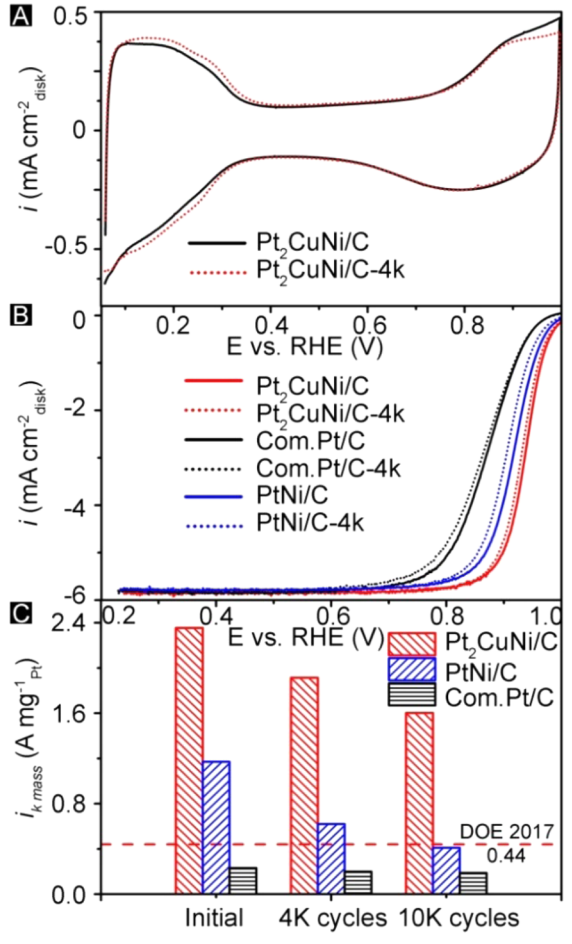

Figure 3. Stability test: (A) CV curves in N_2-protected 0.1 M $HClO_4$ electrolyte and (B) ORR polarization curves in O_2-saturated 0.1 M $HClO_4$ electrolyte before and after 4000 potential cycles, and (C) mass activity of the fresh and after-stability-test catalysts at 0.9 V vs RHE.

DOI: 10.1021/cs502112g
ACS Catal. 2015, 5, 2296−2300

$E_{1/2}$ was limited to less than 10 mV (Figure 3B), suggesting a good stability of the catalyst. The Tafel slopes before and after the test were almost identical, indicating no alternations in the reaction pathway (Figure S10). The $i_{k,\ area}$ and $i_{k,\ mass}$ after the test were 5.19 mA/cm^2 Pt and 1.91 A/mg Pt at 0.9 V versus RHE, representing 22.0% and 18.7% losses specifically. The mass activity loss was significantly less than that for the octahedral PtNi/C (47.0%) and approached to that for the commercial Pt/C (14.3%). After an even longer stabiliy test of 10 000 potential sweeping cycles, the octahedral Pt_2CuNi/C exhibited 4.78 mA/cm^2 Pt and 1.60 A/mg Pt (Figure 3C, SI Figures S5 and S6). It indicated a 31.9% loss in $i_{k,\ mass}$, which again was much less than a 65.0% loss for the PtNi/C. The results indicated a dramatic improvement in stability of the octahedral Pt_2CuNi/C. Moreover, the 1.60 A/mg Pt for the after-test Pt_2CuNi/C was still around 1 order of magnitude higher than the 0.17 A/mg Pt for after-test commercial Pt/C and far exceeded the DOE 2017 target (0.44 A/mg Pt).

The much improved stability of the octahedral Pt_2CuNi/C with respect to the octahedral PtNi/C was further studied by characterizations of the tested catalysts (Figure 4). No observable size variations were found for the Pt_2CuNi particles after 4000 cycles of potential cycling, which was consistent with the small ECSA change. Interestingly, a big portion of the particles maintained their octahedral morphology and smooth edges, confirming good stability of these particles. Representative EDX line scans of individual reacted particles are shown in Figure 4C. Different from an even distribution of Pt, Cu, and Ni in fresh Pt_2CuNi (SI Figure S7), the Pt element exhibited a broader line than both Cu and Ni, suggesting the formation of thin Pt surface layer during the stability test.[6,36] EDX line scans of smaller reacted particles showed similar results (Figure S11), indicating the thin Pt surface layer formation is independent of the Pt_2CuNi size. EDX quantitative analyses of the reacted Pt_2CuNi/C provided more details on the particle composition at different stages. An immediate composition change, from $Pt_{50}Cu_{26}Ni_{24}$ to $Pt_{57}Cu_{25}Ni_{18}$, was observed during the short electrode activation process, probably associated with dissolution of the two elements in the surface region.[17] The composition evolved gradually to $Pt_{62}Cu_{24}Ni_{14}$ after 4k potential cycles and further to $Pt_{64}Cu_{24}Ni_{12}$ after 10k cycles, accompanied by the ORR activity decay. XRD characterization of the Pt_2CuNi/C after 4k potential cycles showed negative shifts in position of the diffraction peaks, caused by the Ni leaching. The lattice parameter determined from the (111) diffraction peak using the Bragg's law was 3.85 Å. The value was between that for fresh Pt_2CuNi/C (3.77 Å) and that for pure Pt (3.93 Å), consistent with the change in alloy composition. Considering the core−shell like characteristic of the tested Pt_2CuNi and that Pt has a larger lattice, the lattice in the thin Pt surface layers was compressed and imposed a strain effect, which could be beneficial for both activity and stability of the catalyst.[32,37,38] In comparison, the poor stability of octahedral PtNi/C was associated with a much faster Ni leaching process and a morphology loss of the particles (SI Figures S8 and S9). Similar findings have been reported in previous studies, with porous and concaved Pt−Ni structures resulting due to Ni leaching.[4,6] The instability of octahedral PtNi/C can be attributed to tunneling Ni dissolution due to segregational element distribution in the nanoparticles, which destabilizes the particles and causes morphology collapse of the particles, leading to rapid activity decay. In comparison, the significantly better stability of the PtCu/C (SI Figure S5E), in consistence with previous studies,[17] benefits from the uniform elemental distribution. The uniform alloy composition helps with intact Pt surface layer formation after Cu in the surface region dissolves and slows down the leaching of Cu in deeper regions. Similarly, the even element distribution in the octahedral Pt_2CuNi uniform alloy nanoparticles ensures the formation of an intact Pt surface layer after the surface region Ni and Cu dissolve. The Pt layer suppresses further dissolution of the two elements in the inner layers and helps to maintain the octahedral morphology, both of which contribute to an improved catalyst stability.

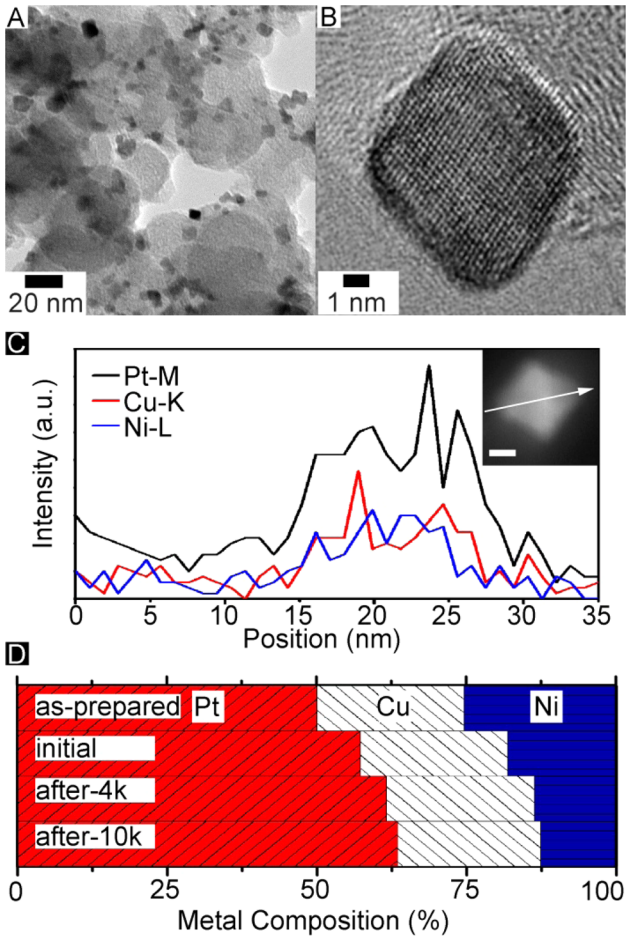

Figure 4. (A) TEM, (B) HRTEM, and (C) HAADF-STEM (scale bar equal to 4 nm) and EDX elemental line scans of the Pt_2CuNi/C after 4000 potential cycles, and (D) composition of the Pt_2CuNi/C at different stages during the stability test.

In summary, we prepared octahedral Pt_2CuNi/C uniform alloy nanoparticle catalyst using a one-step solid-state chemistry approach. The catalyst exhibited both excellent ORR mass activity of 2.35 A/mg Pt at 0.90 V versus RHE and promising stability, with 81.3% and 68.1% retained activity after 4000 and 10 000 cycles of stability test. The values make the octahedral Pt_2CuNi/C a significantly more stable catalyst than the octahedral PtNi/C, which retained only 52.9% and 35.0% of the initial mass activity after the two tests. The outstanding activity of the octahedral Pt_2CuNi/C is the result of combinational electronic and geometric effects, with both optimized d-band center and the (111) surface geometry contributing to boosted ORR kinetics. The much improved stability was attributed to a uniform alloy composition of the

DOI: 10.1021/cs502112g
ACS Catal. 2015, 5, 2296−2300

ternary nanoparticles, which slowed down the leaching process of Ni and Cu and helped to preserve the octahedral morphology. The finding provides insights on factors determining the particle stability and offers guidance on development of highly active and stable ORR catalyst for real applications.

■ ASSOCIATED CONTENT

Supporting Information

The following file is available free of charge on the ACS Publications website at DOI: 10.1021/cs502112g.

Experimental details for preparation, characterization, and testing of the octahedral Pt_2CuNi/C as well other samples, including EDX, TG, XRD, TEM, CV, and LSV data (PDF)

■ AUTHOR INFORMATION

Corresponding Author

*E-mail: zpeng@uakron.edu.

Notes

The authors declare no competing financial interest.

■ ACKNOWLEDGMENTS

This work was supported by the University of Akron start-up fund (Z.P.). The HRTEM data were obtained at the (cryo) TEM facility at the Liquid Crystal Institute, Kent State University, supported by the Ohio Research Scholars Program Research Cluster on Surfaces in Advanced Materials. The authors thank Dr. Min Gao for technical support with the TEM experiments.

■ REFERENCES

(1) Debe, M. K. *Nature* **2012**, *486*, 43−51.
(2) Chen, C.; Kang, Y.; Huo, Z.; Zhu, Z.; Huang, W.; Xin, H. L.; Snyder, J. D.; Li, D.; Herron, J. A.; Mavrikakis, M.; Chi, M.; More, K. L.; Li, Y.; Markovic, N. M.; Somorjai, G. A.; Yang, P.; Stamenkovic, V. R. *Science* **2014**, *343*, 1339−1343.
(3) Stamenkovic, V. R.; Fowler, B.; Mun, B. S.; Wang, G.; Ross, P. N.; Lucas, C. A.; Marković, N. M. *Science* **2007**, *315*, 493−497.
(4) Carpenter, M. K.; Moylan, T. E.; Kukreja, R. S.; Atwan, M. H.; Tessema, M. M. *J. Am. Chem. Soc.* **2012**, *134*, 8535−8542.
(5) Choi, S.-I.; Xie, S.; Shao, M.; Odell, J. H.; Lu, N.; Peng, H.-C.; Protsailo, L.; Guerrero, S.; Park, J.; Xia, X.; Wang, J.; Kim, M. J.; Xia, Y. *Nano Lett.* **2013**, *13*, 3420−3425.
(6) Cui, C.; Gan, L.; Heggen, M.; Rudi, S.; Strasser, P. *Nat. Mater.* **2013**, *12*, 765−771.
(7) Wu, J.; Zhang, J.; Peng, Z.; Yang, S.; Wagner, F. T.; Yang, H. *J. Am. Chem. Soc.* **2010**, *132*, 4984−4985.
(8) Wu, Y.; Cai, S.; Wang, D.; He, W.; Li, Y. *J. Am. Chem. Soc.* **2012**, *134*, 8975−8981.
(9) Choi, S.-I.; Xie, S.; Shao, M.; Lu, N.; Guerrero, S.; Odell, J. H.; Park, J.; Wang, J.; Kim, M. J.; Xia, Y. *ChemSusChem* **2014**, *7*, 1476−1483.
(10) Zhang, C. L.; Hwang, S. Y.; Peng, Z. M. *J. Mater. Chem. A* **2014**, *2*, 19778−19787.
(11) Zhang, C.; Hwang, S. Y.; Peng, Z. *J. Mater. Chem. A* **2013**, *1*, 14402−14408.
(12) Zhang, C.; Hwang, S. Y.; Trout, A.; Peng, Z. *J. Am. Chem. Soc.* **2014**, *136*, 7805−7808.
(13) Denton, A. R.; Ashcroft, N. W. *Phys. Rev. A: At., Mol., Opt. Phys.* **1991**, *43*, 3161−3164.
(14) Zafeiratos, S.; Piccinin, S.; Teschner, D. *Catal. Sci. Technol.* **2012**, *2*, 1787−1801.
(15) Barrett, C. S.; Massalski, T. B. *Structure of metals*; McGraw-Hill: New York, 1966; Vol. *631*.
(16) Cui, C.; Gan, L.; Neumann, M.; Heggen, M.; Roldan Cuenya, B.; Strasser, P. *J. Am. Chem. Soc.* **2014**, *136*, 4813−4816.
(17) Yang, R.; Leisch, J.; Strasser, P.; Toney, M. F. *Chem. Mater.* **2010**, *22*, 4712−4720.
(18) Greeley, J.; Nørskov, J. K.; Mavrikakis, M. *Annu. Rev. Phys. Chem.* **2002**, *53*, 319−348.
(19) Wang, D.; Xin, H. L.; Hovden, R.; Wang, H.; Yu, Y.; Muller, D. A.; DiSalvo, F. J.; Abruña, H. D. *Nat. Mater.* **2013**, *12*, 81−87.
(20) Zhang, Y.; Hsieh, Y.-C.; Volkov, V.; Su, D.; An, W.; Si, R.; Zhu, Y.; Liu, P.; Wang, J. X.; Adzic, R. R. *ACS Catal.* **2014**, *4*, 738−742.
(21) Zhang, S.; Zhang, X.; Jiang, G.; Zhu, H.; Guo, S.; Su, D.; Lu, G.; Sun, S. *J. Am. Chem. Soc.* **2014**, *136*, 7734−7739.
(22) Zhang, L.; Iyyamperumal, R.; Yancey, D. F.; Crooks, R. M.; Henkelman, G. *ACS Nano* **2013**, *7*, 9168−9172.
(23) Zhang, J.; Yang, H.; Fang, J.; Zou, S. *Nano Lett.* **2010**, *10*, 638−644.
(24) Yu, T.; Kim, D. Y.; Zhang, H.; Xia, Y. *Angew. Chem., Int. Ed.* **2011**, *50*, 2773−2777.
(25) Wang, J. X.; Inada, H.; Wu, L.; Zhu, Y.; Choi, Y.; Liu, P.; Zhou, W.-P.; Adzic, R. R. *J. Am. Chem. Soc.* **2009**, *131*, 17298−17302.
(26) Wang, C.; Chi, M.; Li, D.; Strmcnik, D.; van der Vliet, D.; Wang, G.; Komanicky, V.; Chang, K.-C.; Paulikas, A. P.; Tripkovic, D.; Pearson, J.; More, K. L.; Markovic, N. M.; Stamenkovic, V. R. *J. Am. Chem. Soc.* **2011**, *133*, 14396−14403.
(27) Takenaka, S.; Hirata, A.; Tanabe, E.; Matsune, H.; Kishida, M. *J. Catal.* **2010**, *274*, 228−238.
(28) Mazumder, V.; Chi, M.; More, K. L.; Sun, S. *J. Am. Chem. Soc.* **2010**, *132*, 7848−7849.
(29) Chen, Y.; Liang, Z.; Yang, F.; Liu, Y.; Chen, S. *J. Phys. Chem. C* **2011**, *115*, 24073−24079.
(30) Cai, Y.; Adzic, R. R. *Adv. Phys. Chem.* **2011**, *2011*, 1−16.
(31) Loukrakpam, R.; Luo, J.; He, T.; Chen, Y.; Xu, Z.; Njoki, P. N.; Wanjala, B. N.; Fang, B.; Mott, D.; Yin, J.; Klar, J.; Powell, B.; Zhong, C.-J. *J. Phys. Chem. C* **2011**, *115*, 1682−1694.
(32) Strasser, P.; Koh, S.; Anniyev, T.; Greeley, J.; More, K.; Yu, C.; Liu, Z.; Kaya, S.; Nordlund, D.; Ogasawara, H.; Toney, M. F.; Nilsson, A. *Nat. Chem.* **2010**, *2*, 454−460.
(33) Greeley, J.; Stephens, I. E. L.; Bondarenko, A. S.; Johansson, T. P.; Hansen, H. A.; Jaramillo, T. F.; Rossmeisl, J.; Chorkendorff, I.; Nørskov, J. K. *Nat. Chem.* **2009**, *1*, 552−556.
(34) Stamenkovic, V.; Mun, B. S.; Mayrhofer, K. J. J.; Ross, P. N.; Markovic, N. M.; Rossmeisl, J.; Greeley, J.; Nørskov, J. K. *Angew. Chem., Int. Ed.* **2006**, *45*, 2897−2901.
(35) Gasteiger, H. A.; Kocha, S. S.; Sompalli, B.; Wagner, F. T. *Appl. Catal., B* **2005**, *56*, 9−35.
(36) Kang, Y.; Snyder, J.; Chi, M.; Li, D.; More, K. L.; Markovic, N. M.; Stamenkovic, V. R. *Nano Lett.* **2014**, *14*, 6361−6367.
(37) Shao, M.; Odell, J. H.; Peles, A.; Su, D. *Chem. Commun.* **2014**, *50*, 2173−2176.
(38) Gan, L.; Yu, R.; Luo, J.; Cheng, Z.; Zhu, J. *J. Phys. Chem. Lett.* **2012**, *3*, 934−938.

DOI: 10.1021/cs502112g
ACS Catal. 2015, 5, 2296−2300